Master's thesis
Meteorology

Stable boundary layer and katabatic flow inside a boreal forest canopy with sloping terrain

Tuukka Keränen

March 29, 2021

Supervisors: Ph.D. Olli Peltola
Professor Timo Vesala

Examiners: Professor Timo Vesala
Docent Ivan Mammarella

University of Helsinki
Master's Programme in Atmospheric Sciences

P.O. Box 42 (Gustaf Hällströmin katu 2)
FI-00014 University of Helsinki

HELSINGIN YLIOPISTO — HELSINGFORS UNIVERSITET — UNIVERSITY OF HELSINKI

Tiedekunta — Fakultet — Faculty	Koulutusohjelma — Utbildningsprogram — Degree programme
Faculty of Science	Master's Programme in Atmospheric Sciences

Tekijä — Författare — Author

Tuukka Keränen

Työn nimi — Arbetets titel — Title

Stable boundary layer and katabatic flow inside a boreal forest canopy with sloping terrain

Opintosuunta — Studieinriktning — Study track

Meteorology

Työn laji — Arbetets art — Level	Aika — Datum — Month and year	Sivumäärä — Sidantal — Number of pages
Master's thesis	March 29, 2021	40

Tiivistelmä — Referat — Abstract

A stably stratified layer is often observed to form near the surface during nighttime. If the terrain is not flat, cold air near the surface can start to flow down the slope despite the wind direction above the stable layer being different. This slope flow is called katabatic wind. Katabatic winds are challenging for eddy covariance measurements that are commonly used to calculate the fluxes of gases and energy between the soil and the atmosphere. If the measurement is done above the canopy, the katabatic wind may lead to significant advective transport of gas and energy not detected by the measurement. Therefore eddy covariance measurements might underestimate the fluxes by a significant amount. Therefore it is important to understand the mechanisms of katabatic flow so that the effects of it can be taken into account when eddy covariance measurements are used in sloping terrain. This thesis determines how the katabatic flow within a boreal forest canopy in Hyytiälä, Finland depends on the static stability and depth of the stable layer within the canopy. The measurements are also compared to a simplified theory to find out how well the existing formulations of katabatic flow within canopies describe the observed conditions.

Wind measurements done with sonic anemometers and temperature measurements done with distributed temperature sensing system during June-October 2019 are analyzed in this thesis to form understanding of the vertical profiles of temperature and wind within the canopy layer at the measurement site. In addition to the wind and temperature measurements, solar radiation measurements are also used to find the dominant driver for the formation of the stably stratified canopy layer. The measurement site represents typical Finnish Scots pine forest and has sloping terrain with main slope of 2° in the north-south direction.

This study found evidence of katabatic northerly flow forming at the measurement site during stable nights. However, this study could not find a relation between the depth of the stable layer and strength of the katabatic flow. The katabatic flow was observed to get stronger in the open trunk space with increasing static stability within the canopy layer. The results of this study suggest, that katabatic flow follows the simplified theory well within the upper part of the canopy, where the majority of the foliage is. At lower levels within the open trunk space, the simplified model greatly underestimates the flow speed.

Avainsanat — Nyckelord — Keywords

Stable boundary layer, static stability, katabatic wind, boreal forest canopy, DTS

Säilytyspaikka — Förvaringsställe — Where deposited

HELDA - Digital Repository of the University of Helsinki

Muita tietoja — Övriga uppgifter — Additional information

Contents

1. Introduction

Eddy covariance (EC) flux measurement is one of the most progressive methods for measuring ground-atmosphere exchange processes (e.g. Aubinet et al., 2012). It combines many advisable features: EC is direct, ecosystem-scale representative and uninvasive method for estimating the energy and trace gas flux between the soil and the atmosphere (Aubinet et al., 2012). However, one significant problem arises when using EC systems. The ecosystem-atmosphere exchange measurements require the EC sensors to be placed above the vegetation which can lead to information loss about the processes happening inside the vegetation layer within the canopy (Alekseychik et al., 2013). It is very well understood that this loss of information about the processes within the canopy can lead to critical errors in the EC measurements (eg. Staebler and Fitzjarrald, 2004). According to Papale et al. (2006), especially EC measurements conducted at nighttime and in complex terrain can lead to severe underestimation of net ecosystem exchange (NEE). It is trivial, that a large fraction of the Earth has complex terrain with vegetation. This makes it very important to study the possible sources of uncertainty in EC flux measurements (Alekseychik et al., 2013).

The canopy layer flow is observed to fall mostly in two categories: well mixed conditions with turbulence all the way to down to the ground level mostly during daytime, and stably stratified conditions characterized by temperature inversion and suppressed turbulence in the canopy layer mostly during nighttime (Nieuwstadt, 1984). Stable stratification and the weak turbulence production often lead to decoupling of the within-canopy layer from the layer above. This results in the canopy layer falling under control of buoyancy and therefore the flow direction can differ notably from the flow above canopy as it is determined by the topography. This buoyancy-driven nighttime flow is known as katabatic flow and is an essential feature in sloping terrain (e.g. Monti et al., 2002).

Increased interest towards understanding the exchange of energy and carbon between the biosphere and the atmosphere have added motivation to studying the flow inside vegetation canopies. For example, the international FLUXNET program comprises of over 900 eddy-flux towers that measure the land-atmosphere interaction. From the beginning of these studies, starting from the early 1990s, it was clear that there was a substantial lack of understanding the results in cases when the flux towers were situated in a hilly

terrain. In these cases, the 24-hour total measured amount of the net carbon exchange could vary substantially from the stoichiometric limits on photosynthesis and respiration (Finnigan, 2008; Finnigan et al., 2020).

Alekseychik et al. (2013) studied the influence of canopy layer decoupling on the EC measurements in Hyytiälä, southern Finland. Decoupling was observed frequently during summer nighttime, although the height of the decoupled layer varied a lot from near the ground to the top of the canopy. Alekseychik et al. (2013) concluded that decoupling is an important obstacle for EC measurements and the EC sensors can receive the correct information only by chance by irregular turbulence. They suggest that the probability of such lucky mixing event reduces as the decoupling layer deepens. According to Alekseychik et al. (2013), 50 to 100% of the flux information can be lost from EC measurements in decoupling conditions.

Another important motivator for increasing the understanding of flow within stable boundary layers is that ever since the 1990s, numerical weather prediction models (NWPs) are known to have difficulties in presenting stable boundary layers, particularly the near-surface temperature (Sandu et al., 2013). To improve the performance of the models, they are set so that they maintain stronger mixing in stable boundary layers, which, while potentially improving the near-surface temperature forecast, leads to various other problems in weather prediction (Sandu et al., 2013). These problems include the underestimation of the depth of the stable boundary layer, too weak low level jets that are modeled too far from the surface and underestimation of the wind turning within the boundary layer (Bosveld et al., 1999; Brown et al., 2005; Cuxart et al., 2006; Brown et al., 2008; Bosveld et al., 2008; Svensson and Holtslag, 2009). As free troposphere is mostly stable, artificially enhancing the mixing can lead to forecasting errors even well beyond the boundary layer. An example of this is the underestimation of low-level cloud amount (Koehler et al., 2011).

The cold biases of the near-surface temperatures occurring in NWPs during nighttime stable conditions can have various effects. It can lead to for example overestimation of the radiative cooling caused by surface skin temperature, errors related to the horizontal advection, vertical mixing or cloudiness (Sandu et al., 2013). Therefore, there is a need for better understanding of the stable boundary layer physics, so the NWPs could be improved without using the ”nonphysical” method of introducing more mixing within stable boundary layers.

The temperature measurements analysed in this study were conducted using technique called distributed temperature sensing (DTS). DTS systems were first introduced in the 1980s (see e.g. Dakin et al., 1985; Kurashima et al., 1990) and the first applications included fire monitoring, pipeline monitoring and other industrial applications (Tyler et al., 2009). Over the last 10-15 years, many environmental applications have also been

introduced. These include for example borehole observations, groundwater, lake and ice cave observations as well as soil observations (see de Jong et al., 2015 and references therein). It is only in the last decade, during which DTS has been used in atmospheric temperature sensing (see e.g. Keller et al., 2011; Petrides et al., 2011; Thomas et al., 2012, Peltola et al., 2020). The main reason for this is that a lot of effort has been put into overcoming the effect of solar radiation on atmospheric DTS measurements (de Jong et al., 2015).

The aim of this study is to find how the within-canopy katabatic flows at SMEAR-II station in Hyytiälä, southern Finland depend on the depth of the stable layer and the static stability within the canopy. The vertical temperature profile within the canopy was measured continuously during summer 2019 using DTS. Simultaneously, the vertical wind profile, both the speed and direction, were measured next to the temperature measurements. This study utilizes these measurements to find the atmospheric conditions that favor the formation of the nocturnal downslope flow within the canopy. The results are also compared to a previous theory of subcanopy nocturnal flow in sloping terrain by Yi et al. (2005) to investigate, how the theory matches with the measurements in a boreal Scots pine forest. Finally, some possible reasons for the differences between the theory and the measurements are discussed.

2. Theory and background

This chapter covers the basics of atmospheric boundary layer including nocturnal stable boundary layer. Also included in this chapter are the basic physical mechanisms behind slope winds, particularly downslope, or katabatic, wind. A simplified theoretical approach on katabatic wind inside a forest canopy is presented in section 2.2.2. In the final section the theoretical basis of DTS measurements is presented.

2.1 Atmospheric boundary layer

The lowest part of the atmosphere that is directly influenced by the surface of the Earth is known as the atmospheric boundary layer (ABL) (Cushman-Roisin, 2019). The surface affects the properties of the ABL in many ways. Solar radiation plays a key role in affecting the temperature, turbulence and moisture of the ABL. As the surface is heated by solar radiation, the stratification of the air in the stable boundary layer (SBL, discussed in chapter 2.1.1) is no longer stable, which induces turbulence that mixes the air inside the ABL efficiently. The wind velocity in the ABL is affected by the friction of the rough surface (Cushman-Roisin, 2019).

The air in the ABL can be either stably, unstably or neutrally stratified (Garratt, 1994). The vertical gradient of the potential temperature θ describes the so called dry static stability of the air (Kaimal and Finnigan, 1994) and is written as

$$\frac{\partial \theta}{\partial z} = (\frac{\partial T}{\partial z} + \frac{g}{c_p}) \tag{2.1}$$

where $\partial T/\partial z$ is the vertical gradient of temperature, g is the gravitational acceleration and c_p is the specific heat of air in constant pressure. The fraction g/c_p is called the adiabatic lapse rate (Kaimal and Finnigan, 1994).

When the gradient of the potential temperature is zero, the air parcels raised upwards will have the same density as their environment, therefore not accelerating further after displacement, resulting in a neutral stratification. In stable or unstable stratification, the gradients of the potential temperatures are > 0 and < 0, respectively (Kaimal and Finnigan, 1994).

The top of the ABL is usually defined by a stable layer called capping inversion, which separates the boundary layer below from the free atmosphere above. The turbulent motions below the capping inversion are generally unable to penetrate the inversion, although they may weaken it (Garratt, 1994).

The height of the boundary layer can be theoretically formulated. Tennekes (1982) showed, that boundary layer depth is

$$z_h = C\frac{u_*}{f} \tag{2.2}$$

where u_* is friction velocity, f is the Coriolis parameter and C is an empirical constant. However, theoretical definitions make assumptions that are rarely true in the real atmosphere. In reality, the Coriolis and frictional effects are often masked by lapse rate evolution and subsidence, so equation 2.2 cannot necessarily provide reliable estimates of z_h (Kaimal and Finnigan, 1994). The definition in equation 2.2 also assumes neutrally stratified ABL, where the air parcels experience no net buoyancy forces when displaced (Kaimal and Finnigan, 1994). Therefore z_h is much more difficult to estimate reliably in reality than equation 2.2 suggests.

The height of the boundary layer varies with a diurnal cycle, with the ABL being deepest during daytime and shallowest during nighttime (Kaimal and Finnigan, 1994). The daily cycle of the ABL is clearly revealed from the lapse rate evolution during the day (Bianco et al., 2011). Lapse rate in the ABL is nearly constant and typically close to adiabatic during daytime and positive in the nighttime due to radiational cooling of the surface. In locations where the nocturnal lapse rate is small (not strongly positive), the ABL can develop to be much deeper than in the strongly stable case, where the nocturnal lapse rate is strongly positive (Bianco et al., 2011). Subsidence plays an important role especially in the formation of nighttime stable boundary layers, as nights with strong radiative cooling are also most likely to have subsidence (Carlson and Stull, 1986). Subsidence makes the nocturnal boundary layer to develop slower, because the divergence associated with subsidence removes some of the cooled nocturnal boundary layer air. Another way to interpret the effect of subsidence is that the subsidence-induced heating partially compensates the radiative cooling (Carlson and Stull, 1986).

Neutral stratification of the ABL requires that the lapse rate is adiabatic (see equation 2.1), but this kind of lapse rate is often temporary. On the other hand, two more persistent states can be observed (Kaimal and Finnigan, 1994). These states are the daytime convectively mixed boundary layer (CBL) and the nighttime stable boundary layer (SBL), the latter of the two being especially of interest in this study. Nighttime stable boundary layer is discussed more in section 2.1.1.

2.1.1 Stable boundary layer (SBL)

As already mentioned, boundary layer can be also stably stratified. Most commonly, the cause of such stratification is radiative cooling that occurs during nighttime, especially in relatively cloud-free conditions. Other formation mechanisms are also possible, such as when warm air from land flows over a cold water surface. However, there are still some fundamental knowledge gaps in understanding this very common phenomenon (Smedman et al., 1993; Mahrt, 2014).

The radiative cooling of the surface gives rise to a vertical temperature gradient and heat transfer from the warmer air to the cooler ground surface. This heat transfer from the air to the ground then causes the air close to the ground to cool down, which leads to stable stratification and an inversion layer (Mahrt, 2014). An inversion means that the air temperature rises when moving upwards, thus being "inversely" stratified. The cooling of the air is greatest when the sky is clear, the air is dry and clean. The more dry the soil is, the smaller its thermal conductivity is and therefore more efficient the cooling of the ground surface is (Mahrt, 2014). The development of the SBL can begin before the sunset, when the net radiative cooling becomes greater than the incoming solar radiation. SBL can survive for even several hours after sunrise and even through the whole day, especially in winter conditions as the maximum of solar radiation is relatively weak due to the low sun angle (Mahrt, 2014).

Stable boundary layers can be vertically divided into four sublayers. These include, from the ground up, the roughness sublayer, surface layer, outer layer and entrainment layer where the boundary layer is entrained into the free atmosphere (Mahrt, 2014). These layers are idealizations based on similarity theory and are applicable to only weakly stable boundary layers. There is no such theory for very stable boundary layers. In addition, similarity theory is not typically used in the lowest part of the boundary layer, the roughness sublayer (Mahrt, 2014). This is because there the individual roughness elements such as buildings in urban areas and trees in rural areas affect the flow greatly (Finnigan, 2000).

The layer over the roughness sublayer, the surface layer, can be usually expressed in terms of the Monin-Obukhov similarity theory. In Monin-Obukhov theory the relationship between the flux and the gradient of some arbitrary variable F is expressed as (Mahrt, 2014)

$$\phi_F \equiv \frac{\kappa z \partial \overline{F}/\partial z}{F_*} \tag{2.3}$$

where time average is denoted by overbar, κ is the von Karman constant and z is height above ground. $F_* = |\overline{w'F'}|/u_*$ where $\overline{w'F'}$ is the surface flux of F and u_* is the friction velocity. The apostrophe marks deviation from mean state. The nondimensional gradient

(ϕ_F) is a function of stability

$$\phi_F = f(z/L) \tag{2.4}$$

where z/L is called the stability function and L is the Obukhov length

$$L \equiv -u_*^3\overline{\theta}/(\kappa g\overline{w'\theta'}) \tag{2.5}$$

where $\overline{w'\theta'}$ is the surface heat flux. The stability function describes the decrease of turbulence with increasing stabilities. Greater stability leads to large z/L and smaller flux for a given vertical gradient (Mahrt, 2014).

Determining the depth of the SBL is not straightforward, and no solution really exists which is proven to work well in all situations (Seibert et al., 2000). There were mainly three options that could be considered in this study.

The depth of the SBL can be approximated by determining the level where the gradient Richardson number Ri_g or the bulk Richardson number Ri_B exceeds a critical value (Zilitinkevich and Baklanov, 2002). A second option could be to use the height of the maximum value of static stability within the canopy. The third option, that was finally chosen to be used, is to determine the depth of the SBL as the level at which the standard deviation of temperature exceeds a threshold value.

2.1.2 Flow within forest canopy

The existing similarity theory discussed in the previous section is not expected to be valid within the canopy layer, because there the fluxes vary quickly with height related to sinks and sources of momentum and heat within the canopy (Mahrt et al., 2000). The surface fluxes may not establish equilibrium with the air within the canopy because occasionally turbulence of relatively large scale can penetrate from above into the subcanopy layer (Baldocchi and Meyers, 1991). E.g. Sun et al. (1998) and Gao et al. (1989) provide further details on the penetration of gusts into the canopy layer. Simultaneously, part of the subcanopy flux can happen on very small scales that may not be completely resolved by sonic anemometers. Therefore the subcanopy turbulence is comprised of both penetrating eddies and local small-scale eddies and the appropriate length scale for the similarity theory is not clear, which makes the application of the theory difficult (Mahrt et al., 2000).

These difficulties make the observational support for the formulations of within-canopy fluxes rather lean, and this especially holds for the nocturnal case (Mahrt et al., 2000) that is the most important in this study. Strongly stable conditions above the canopy can cause the the flow within the canopy to get decoupled from the flow above. In nighttime, when stable conditions are common, this helps the formation of katabatic flows

(Launiainen et al., 2007), that are discussed more in section 2.2.1. Katabatic flow is a major issue in the interpretation of nocturnal fluxes of for example CO_2 that are measured above the canopy and linked to long term ecosystem carbon sequestration (Aubinet et al., 2003; Feigenwinter et al., 2004; Staebler and Fitzjarrald, 2004; Yi et al., 2005). Launiainen et al. (2007) showed that in Hyytiälä, a secondary wind speed maximum in the lower part of the canopy layer develops during stable conditions within the canopy and generally gets stronger with increasing stability. They suggest, that one reason for the lower secondary wind maximum could be due to katabatic flow.

2.2 Slope winds

The phenomenon of slope wind is discussed in this section. Firstly, the basic physical mechanisms of slope winds are discussed in section 2.2. Secondly, section 2.2.1 focuses on nighttime airflow in sloping terrain known as katabatic wind. Finally, section 2.2.2 focuses on a previous study by Yi et al. (2005), where a combination of simulation and experiments were used to formulate a theoretical representation of katabatic wind inside a forest canopy.

Flows along a slope have an important role in the diurnal circulation of regions with complex terrain such as mountains and valleys. These flows are caused by thermal forcing acting on the complex topographic surfaces and are part of winds known as thermal circulation (Monti et al., 2002). These thermal circulation flows can have scales from a few kilometers or less to even hundreds of kilometers (Bossert and Cotton, 1994). Slope flows are caused by the difference in air temperature between air close to the slope surface and the air at the same altitude further away from the slope. This temperature difference is driven by heating during the daytime and cooling during nighttime (Monti et al., 2002).

During the day, the flow is directed typically upslope and is known as anabatic flow. During nighttime the flow is downslope, also known as katabatic flow (Monti et al., 2002). According to Papadopoulos and Helmis (1999) sustained wind speeds of about 1-5 m/s are characteristic for these flows along a slope and the transition between anabatic and katabatic flows during morning and afternoon is characterised by periods of significantly low winds of <1 m/s. These low wind periods reduce the dispersion and transport near the ground, which can lead to accumulation of pollutants and therefore worsen the air quality significantly in areas with complex terrain (Whiteman, 2000).

Katabatic and anabatic flows have been studied in various studies using field experiments under different conditions. Some examples include extreme conditions such as Antarctica (e.g. Lied, 1964) and calmer conditions over gentle slopes (e.g. Mahrt, 1990). Natural variability of for example the slope angle and direction makes it difficult to control the field conditions, so more recently slope flows have been studied using modelling

(Monti et al., 2002). With models it is easy to construct idealised environments where the parameters are more under control than in nature. One such study by Yi et al. (2005) is introduced more thoroughly in section 2.2.2.

2.2.1 Katabatic wind

Downslope winds, or in other words katabatic winds, develop when stable boundary layer (SBL) forms over a sloping surface (Stiperski et al., 2020). Favourable locations include valleys, mountains or even small hills with elevation of only a couple of tens of meters, as is the case in this study. The flow is formed when surface cooling makes the air near the surface cooler and less buoyant than the air further away from the surface (Stiperski et al., 2020). Gravity then causes the air near the surface to start flowing in the direction of the steepest slope and causes a low level wind maximum.

Katabatic flows are generally quite weak in the midlatitudes, where the flows are of the order of some m/s. In Antarctica, however, katabatic flows can intensify due to steepening terrain and converging flows, reaching speeds of over 50 m/s and have significant effect on the local climate (Parish and Bromwich, 1989).

Studies on the mean structure of katabatic flows (e.g. Monti et al., 2002) have shown that the wind maximum tends to form in the middle third of the surface-based inversion layer, so not at the top or at the bottom. Of course, this also depends on how the height of the inversion layer is defined, as according to Stiperski et al. (2020) it can be done based on wind speed, flux or temperature profiles as in this study. It is also important to note, that most of the previous studies are focused on deeper katabatic flows, where the flow maximum can be even several tens of meters above ground. This study focuses on shallower flow and the maximum was mostly observed under ten meters above ground.

2.2.2 A simplified theory on katabatic flow inside a forest canopy

Several theoretical and experimental attempts have been made to formulate the flow inside forest canopies in sloping terrain. This section mainly focuses on a study by Yi et al. (2005), which combines modeling and measuring of the katabatic flow inside a canopy with complex terrain.

Yi et al. (2005) measured drainage flows inside a subalpine forest canopy with a maximum tree height of 16 m. The measurement site was located in the Niwot Ridge Ameriflux site in the Rocky Mountains, Colorado, US. The measurement site included four towers aligned approximately in the east-west and north-south directions, with westerly wind component known to dominate the nocturnal katabatic flow. Eddy covariance fluxes

of water vapor, CO_2 and sensible heat were measured on the east-west aligned towers. For more detailed description of the measurement site, see Yi et al. (2005).

Yi et al. (2005) assumed a stable, incompressible and inviscid atmosphere, where the katabatic flow is assumed to develop over a slope with a constant angle α. Cartesian coordinates were used, with x in the direction of the katabatic flow and z normal to the slope. The canopy is assumed to have a horizontally uniform structure but variation in the vertical is allowed. It is important to note, that in reality the canopy does always have some horizontal variation. Vertical motion and horizontal pressure gradient are not considered and Coriolis force is neglected. These simplifications are reasonable, as the scale of the flow is small for them to act significantly. Considering steady state, Yi et al. (2005) used a definition by Wilson and Shaw (1977) and Mahrt (1982):

$$-\frac{\partial \overline{u'w'}}{\partial z} - g\frac{\Delta\theta}{\theta_0}\sin\alpha = c_D(z)l(z)u^2(z) \tag{2.6}$$

where $-\overline{u'w'}$ is the shear stress, θ_0 is the ambient potential temperature, $\Delta\theta$ is the difference in potential temperature in the katabatic flow, $l(z)$ is leaf area density facing the mean wind, $c_D(z)$ is the effective drag coefficient of the canopy elements and $u(z)$ is the mean wind velocity. Apostrophes denote deviation from mean state. Yi et al. (2005) defined the drag coefficient according to Mahrt et al. (2000) as

$$c_D(z) = \frac{u_*^2(z)}{u^2(z)} \tag{2.7}$$

where $u_*(z)$ is the friction velocity inside the canopy that is related to shear stress:

$$-\overline{u'w'} = u_*^2(z). \tag{2.8}$$

After substitution, equation 2.6 can be expressed as

$$\frac{\partial(c_D(z)u^2(z))}{\partial z} - c_D(z)u^2(z)l(z) = g\frac{\Delta\theta}{\theta_0}\sin\alpha. \tag{2.9}$$

After multiplying both sides of equation 2.9 by $e^{-A(z)}$ where $A(z)$ is the cumulative leaf area below height z

$$A(z) = \int_0^z l(z')dz' \tag{2.10}$$

and integrating within the canopy from height z to the top of the canopy, h, equation 2.9 becomes

$$u^{\pm}(z) = \pm(e^{-(LAI-A(z))}\frac{c_D^h}{c_D(z)}u_h^2 - g\frac{\Delta\theta\sin\alpha}{\theta_0 c_D(z)}\int_z^h e^{-(A(z')-A(z))}dz')^{\frac{1}{2}}, \tag{2.11}$$

where $A(h) = LAI$ is the one-sided leaf area index, u_h is the wind speed at the top of the canopy and c_D^h is the drag coefficient at the top of the canopy.

Yi et al. (2005) state that equation 2.11 is the first analytical solution to slope wind inside a forest canopy. In their solution, both the upslope (-) and downslope (+) winds are covered. This study will focus solely on the downslope part, as that is relevant for the nocturnal flow.

One simplification of the model by Yi et al. (2005) was the assumed uniformly distributed leaf area $l(z) = l = const.$ The other important assumption by Yi et al. (2005) was that the drag coefficient is constant. These assumptions reduce equation 2.11 to

$$u(z) = (\frac{c_D^h u_h^2}{c_D} e^{-LAI(1-\frac{z}{h})} - \frac{gh\Delta\theta \sin\alpha}{\theta_0 LAI c_D}(1 - e^{-LAI(1-\frac{z}{h})}))^{\frac{1}{2}}, \tag{2.12}$$

where

$$\frac{A(z)}{A(h)} = \frac{z}{h}, l(z) = \frac{LAI}{h}$$

were used. The wind below the canopy ($u(z)$) in equation 2.12 by Yi et al. (2005) can be partitioned into slope-dependent and slope-independent components:

$$u(z)^2 = u_f^2 + u_g^2. \tag{2.13}$$

The slope-independent component is parallel to the wind above the canopy and can be written as

$$u_f(z) = \sqrt{\frac{c_D^h}{c_D}} u_h e^{-\frac{LAI}{2}(1-\frac{z}{h})}. \tag{2.14}$$

Equation 2.14 is the exponential model for wind within a canopy (Inoue, 1963; Cionco, 1965; Cowan, 1968; Cionco, 1972; Raupach and Thom, 1981; Albini, 1981; Wilson et al., 1982; Massman, 1987; Macdonald, 2000; Mohan and Tiwari, 2004). Using the same simplifications and assumptions, the slope-dependent wind component is written as

$$u_g(z) = \sqrt{-\frac{gh\Delta\theta \sin\alpha}{\theta_0 LAI c_D}(1 - e^{-LAI(1-\frac{z}{h})})}. \tag{2.15}$$

As the drag coefficient was assumed to be constant in the vertical direction, equation 2.14 is reduced to

$$u_f(z) = u_h e^{-\frac{LAI}{2}(1-\frac{z}{h})} \tag{2.16}$$

where u_h is the wind speed at the top of the canopy and z is the measurement height below the canopy. From equation 2.15 it is important to notice that u_g is zero, if the

canopy is neutrally stratified ($\Delta\theta = 0$) or if the surface is horizontal ($\alpha = 0$). In those cases, the wind within the canopy equals u_f. For the case in Hyytiälä considered in this study, the one-sided leaf area index was set to 4 $\mathrm{m^2 m^{-2}}$, the all-sided leaf area index being 8 $\mathrm{m^2 m^{-2}}$. If $\vec{u}$ is known from measurements, then the slope-dependent component $\vec{u}_g$ can also be calculated as a difference between $\vec{u}$ and $\vec{u}_f$ vectors as

$$\begin{aligned} \vec{u}_g &= \vec{u} - \vec{u}_f \\ \vec{u}_g &= (|\vec{u}| \sin a - |\vec{u}_f| \sin b)\vec{i} + (|\vec{u}| \cos a - |\vec{u}_f| \cos b)\vec{j} \end{aligned} \tag{2.17}$$

where a is the wind direction at height z, b is the wind direction at top of the canopy and u_f was defined to be parallel with the above-canopy flow. The direction of $\vec{i}$ is parallel to the above-canopy flow and $\vec{j}$ is perpendicular to it. The slope-dependent wind speed can be solved from 2.17 as the length of the vector:

$$u_g(z) = \sqrt{(|\vec{u}| \sin a - |\vec{u}_f| \sin b)^2 + (|\vec{u}| \cos a - |\vec{u}_f| \cos b)^2} \tag{2.18}$$

2.3 Theoretical basis of distributed temperature sensing (DTS)

Many atmospheric processes such as turbulence and structure of the boundary layer span spatial scales from millimeters to kilometers, which presents challenges for observing, describing and modeling of these processes. Considering only observation of temperature, most conventional *in situ* temperature measurement systems measure data representing a sphere of some small diameter centered around a measurement point (Selker et al., 2006). This means that in principle, it would be possible to observe processes across wide range of scales if one would place these measurement sensors close to each other across some area of interest. However, this approach would soon become too exhausting and impractical as the amount of sensors would soon exceed any reasonable number. Even if one would have the patience and budget to set up such system, the closely spaced sensors would very likely disturb the airflow around each other and also the errors between the sensors can be large compared to the actual differences in temperature (Selker et al., 2006).

DTS allows temperature measurements continuously along optical fibers (de Jong et al., 2015). The DTS measurement system consists of an optical fiber, a laser, a detector and a computer with software that calculates and visualizes the measured temperature as well as collects and saves the data.

The temperature sensing is based on the backscattering of laser pulses sent through an optical fiber (de Jong et al., 2015). Analysis of the Raman spectrum of the backscat-

tering makes the calculation of the temperature possible, and the time of flight of the laser pulse gives the position on the fiber from where the temperature was measured (de Jong et al., 2015).

When hitting matter, light can be reflected at the original wavelength, or a part of the light can be adsorbed and re-emitted at wavelengths that are slightly below or above the original wavelength of the incident light. The change in the wavelength arises from the loss or gain of energy quanta that are exchanged with electrons. This wavelength-shifted reflected light is called Raman scattering (Selker et al., 2006). The light with wavelength longer than that of the incident light is called Stokes backscatter and the light with wavelength shorter than that of the incident light is called anti-Stokes backscatter (Selker et al., 2006).

Raman Stokes backscattering depends linearly on the intensity of the illumination below a critical light intensity (Selker et al., 2006). At the same intensities the anti-Stokes backscattering depends on the intensity of illumination and is additionally exponentially dependent on the temperature of the fiber (Selker et al., 2006). The ratio between the magnitudes of the anti-Stokes and Stokes backscattering is therefore independent of the illumination intensity and only leaves the exponential temperature dependence (Selker et al., 2006).

The precision of Raman-based measurement is limited by the standard deviation of the ratio between anti-Stokes and Stokes signals (Selker et al., 2006). The standard deviation follows a normal distribution, decreasing with the square root of the total amount of observed photons. Therefore the precision of the temperature measurement will increase with the square root of the integration interval of the instrument (Selker et al., 2006). The intensity of the light and hence the strength of the measured backscattering signal weakens exponentially with distance according to Beers law (Selker et al., 2006). The instrument will detect lower number of photons from greater distance compared to points closer to the instrument in the same time. The points far from the instrument will therefore need a longer integration time to achieve a desirable precision (Selker et al., 2006).

To summarize, Raman-based measurement's precision is proportional to the square root of the product of the number of the resolved fiber sections and the distance from the instrument divided by the integration time. Selker et al. (2006) state as an example, that the standard deviation of a measurement taken 1 km from the instrument with 1 m spatial resolution and integrated for 1 min will be of the order of 0.1°C, although this value varies depending on the instrument used. Measurements averaged over one hour can reach standard deviation of 0.02°C. The real precision of the measurement system also depends on the measurement setup. It is important to place the optical fiber in a known temperature and take a long-time integration data set. Suitable calibration could

be for example a water bath like in the measurements analysed in this study (Peltola et al., 2020). Hence the absolute precision of each measurement system is usually limited by the accuracy of the calibration more than the accuracy of the instrument itself. Even careful calibration will not remove possible random error, but it can be used to minimize systematic error. On the other hand, longer integration interval does not decrease systematic error but will decrease random error.

Improving the precision of the measurement is not possible by using more powerful lasers. This approach is limited by the fact that the Raman backscattering behaves nonlinearly as the intensity of the light is increased over a certain critical value (Selker et al., 2006). Therefore the intensity must be kept below this threshold in order to not lose precision (Selker et al., 2006).

3. Methods

3.1 Measurement site and instrumentation

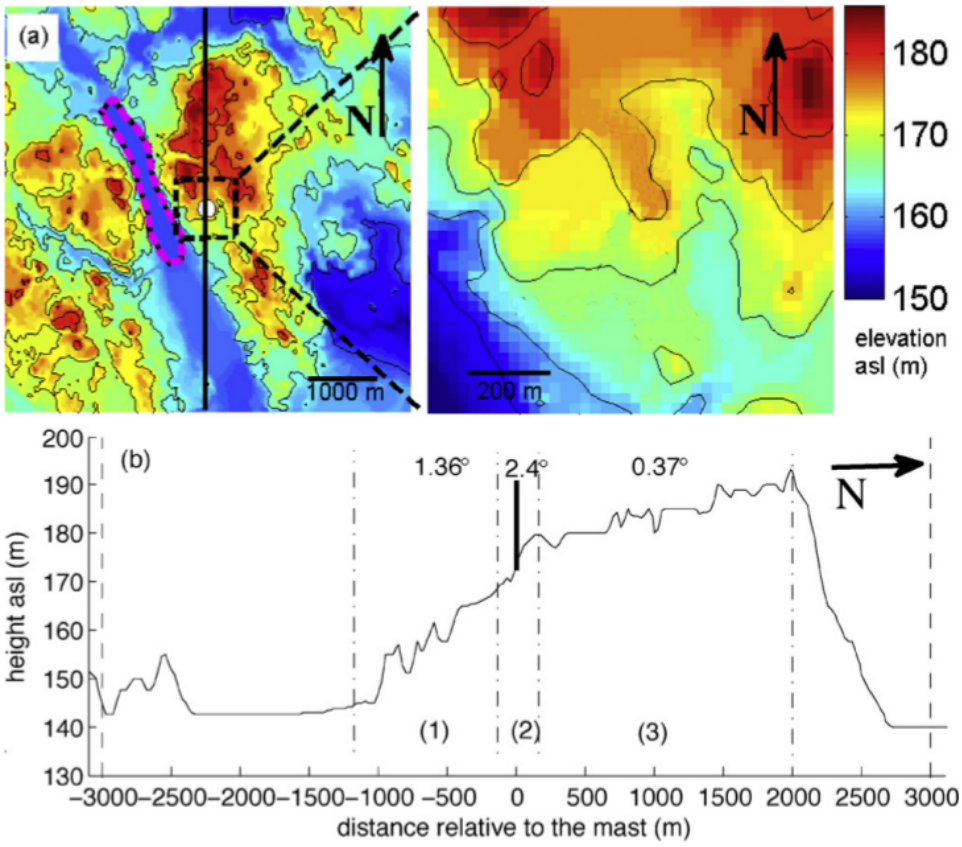

Figure 3.1: (a) The topography of the SMEAR-II station. The station is marked by the white circle at the center. The upper right-hand panel shows a close-up of the area in (a) marked with the dashed black square. The location of the N-S transect (b) is marked by the black vertical line in (a). (b) The N-S transect of topography through the main mast (shown as a vertical line at $x = 0$, not to scale). The hill is divided into three parts by the dash-dot lines according to the prevailing agle of the slope. The distance in x-axis is relative to the mast. Adapted from Alekseychik et al. (2013).

The measurements analysed in this study were collected during a campaign between May and October 2019 in Hyytiälä SMEAR-II station. A wide range of biospheric and atmospheric measurements are collected continuously at the site. The measurement site

is located in central Finland (61.845° N, 24.289° E) and is dominated by Scots pine stand with an average tree height of 17 meters (Peltola et al., 2020). The forest canopy height is 10 to 17 meters and below the canopy there is open trunk space with only few branches. The terrain around the site is suitable for the development of gravity-driven katabatic winds. This is because the site is located on a hill with the main slope of approximately 2° roughly in the north-south direction (Peltola et al., 2020). Figure 3.1 shows the topography of the measurement site in more detail.

Figure 3.2: A photo of the DTS arrangement used in this study. Red lines highlight where the optical fibers are. Red arrows indicate the positions of the 3D anemometers at 1 m and 5.5 m heights and yellow arrow indicates the position of the 2D anemometer at 8.6 m.

The wind speeds at 1 m, 5.5 m, 8 m and 16.8 m were measured using 2D and 3D ultrasonic anemometers. 3D anemometers (USA-1 by METEK GmbH, Germany) providing three wind components at a sampling frequency of 10 Hz were used at 1 m and 5.5 m heights. 2D anemometers (Ultrasonic anemometer 2D by Adolf Thies GmbH & Co. KG) that provided 2 horizontal wind components at sampling frequency of 1/60 Hz were installed at 8 m and 16.8 m heights.

The DTS measurements used in this study were conducted near the 125 meters tall main mast of the station. The instrument itself (Ultima-S, 5 kilometer variant, Silixa Ltd., Hertfordshire, United Kingdom) was placed in a wooden cabin near the main mast. Two calibration baths of about 50 l were installed at the cabin so that the cable ran through both baths in the beginning as well as in the end of the measurement length (Peltola et al., 2020). The temperature of the baths was controlled with two thermostats (RC 6 CS, LAUDA DR. R. WOBSER GMBH & CO. KG, Lauda-Königshofen, Germany). The temperatures of the baths were set at 5 °C and 30 °C, so that the measured air temperature

fell in between the bath temperatures. The temperature in the baths was monitored by PT-100 reference thermometers that were supplied with the DTS instrument and logged with the same instrument with a precision of 0.01 °C. In addition to the external water baths, the device also has its own calibration coil of about 30 meters inside the device (Peltola et al., 2020).

The measuring cable consists of a glass core with aramid fiber reinforcement coated with a white outer housing. The total outer diameter of the cable is 0.9 mm. White cable was used to minimize cable heating due to absorption of solar radiation (Peltola et al., 2020; de Jong et al., 2015) and maximize the high frequency response of the measurements.

The cable route ran through both the baths, then horizontally back and forth between a 26 m tower and the main mast at 18 heights. The lowest measurement height was just above the shrubbery growing on the ground and the highest level was at 21.5 m. Then the cable ran through the calibration baths once more to finish.

The cable was routed around round plastic pots (diameter of approximately 20 cm) at the turning points of each horizontal line. This was done to prevent the cable from sagging and also to avoid sharp edges which can affect the measurement negatively, or in the worst case, even brake the fragile glass fiber running inside the cable (Tyler et al., 2009). Additionally, the cable was routed under wooden blocks that gently pushed the cable against the pot. A photo of the measurement arrangement is shown in figure 3.2.

There are two main issues that affect the measurement at the fastening points: Firstly, if the cable is being pinched too strongly by the wooden block, the signal in the cable will be disturbed as the amount of noise is increased. This will make the signal-to-noise ratio worse, effectively making the measurement less precise (Tyler et al., 2009). Secondly, the reddish-brown colored pots absorb solar radiation and can heat up many degrees warmer than the air around them. This causes unnatural temperature peaks at the locations of the pots. Therefore the data points where the cable was in contact with the fastening pots were all removed before further analysis.

3.2 Data processing

The DTS instrument measured the temperature at 0.127 m spatial resolution and 0.5 Hz temporal resolution in single-ended mode. The temporal statistics (mean and standard deviation) of the temperatures were computed over a 5-minute period. Therefore every full day had 288 data points. The averaging was done to reduce unwanted noise that could affect the analysis. The DTS measurements from the 18 heights were spatially interpolated to a spatial resolution of 0.5 m between 0 m and 21.5 m heights and between the towers providing a 2D spatial grid of air temperature data within the canopy. However, only vertical variability was considered in this study.

The vertical structure of the boundary layer is actually visually very easy to analyse just by looking at the vertical temperature profiles measured by the DTS system. However, computationally it is quite far from being simple. The detection of the inversion height was especially important for successful analysis to be possible in this study. It also proved to be the most difficult one to determine reliably with a code.

After trial and error, the best approach was found to be by determining the depth of the inversion layer as the height of maximum standard deviation of the DTS temperature, with a minimum value to filter moments with no actual inversion. The height of the maximum value of static stability was not used, as it was found to be almost always at ground level or very close to it. Therefore it would not represent the true depth of the inversion layer. The method based on treshold values of either gradient or bulk Richardson number was not used, because previous studies have shown that it can provide only a rough estimate of the SBL depth and should be used with caution in shallow, stably stratified boundary layers (e.g. Seibert et al., 2000; Zilitinkevich and Baklanov, 2002). The minimum value was needed, as a maximum value for the standard deviation is found for all times, but that does not automatically mean that inversion actually exists, or it can be negligibly weak. It was evident that there was a clear correlation between large standard deviation of temperature and the cap of a strong temperature inversion.

Bin averaging method is a pre-processing technique used to reduce the effect of possible random errors in the data values. In this study, bin averaging was used to find out the effect of atmospheric stability and the depth of SBL to the katabatic wind speed. Instead of plotting every value of atmospheric stability or depth of SBL with their corresponding wind speeds, those variables were divided into a few bins that represent different conditions.

The wind speeds were divided into bins by the potential temperature gradient between 1 m and 20 m. Four bins were chosen to represent different strengths of inversion: near neutral (0-1 °C), weakly stable (1-2 °C), moderately stable (2-3 °C) and strongly stable (>4 °C). The temperatures were chosen from heights 1 m and 20 m because they were thought to provide the best representation of the temperature gradient within the canopy.

When analysing the effect of the height of inversion to the katabatic wind speed, the wind speeds were also divided into four bins representing different heights of the inversion: 0-5 m, 5-10 m, 10-15 m and >15 m.

All of the measurements analysed in this study were continuous with no distinction between night and day measurements. This study focuses on phenomena happening during nighttime, so some separation had to be made between what was considered as ”night” and ”day”. This separation was made by considering the time between sunset and sunrise to be night and the remaining time to be day. Sunset and sunrise times were

taken for Orivesi, some 20 kilometers south from the measurement site. If the time of the sunset or sunrise did not exactly meet with the time of the averaging period, closest 5-minute averaging period was chosen as the representative time.

4. Results

The results of the analyses done to the DTS, wind and radiation measurements are presented in this chapter. First, the DTS temperature measurements are compared against reference measurements and their validity is assessed in chapter 4.1. Secondly, the vertical temperature gradients are presented in chapter 4.2. The measured and calculated depth of SBL used for later katabatic wind calculations are compared in chapter 4.2.1. The effect of wind and net radiation to the static stability is presented in chapter 4.2.2.

The analysed katabatic flow speed and direction in varying stability conditions are presented in chapter 4.3. Vertical profiles of katabatic flow in different inversion and atmospheric stability conditions are presented in chapter 4.4. In chapter 4.4.3 the analysis done on katabatic flow based on the measurements is compared with a theoretical approach presented in chapter 2.2.2.

4.1 Validation of the DTS measurements

The main challenge of using DTS in atmospheric applications is reducing the error induced by solar radiation heating the cable warmer than the surrounding air temperature. Increasing the amount of insulation around the fiber could be one way to solve the issue. Traditional thermometers are usually shielded with some kind of a screen. However, in the case of optical fibers, increasing the amount of protective material around the fiber would not solve the problem of solar heating. Instead it would make the measurement of the air temperature even more difficult, as the fiber would be too insulated from the air to measure the temperature reliably. Schilperoort et al. (2018) used a screen gauze around the southern (sunny) side of the cable fixed 15 cm away from the cable. This setup allows for sufficient ventilation around the cable but it also disturbs the flow around the cable too much to measure the turbulent variation (standard deviation) of temperature.

The measurements analysed in this study were carried out with the fiber coated in white. It is very likely that without the use of further data correction, black coating would have resulted in larger error as black cable absorbs more solar radiation.

To verify that the DTS system produced precise temperature readings, the measurements were compared to the data from PT-100 platinum wire thermistors. The ther-

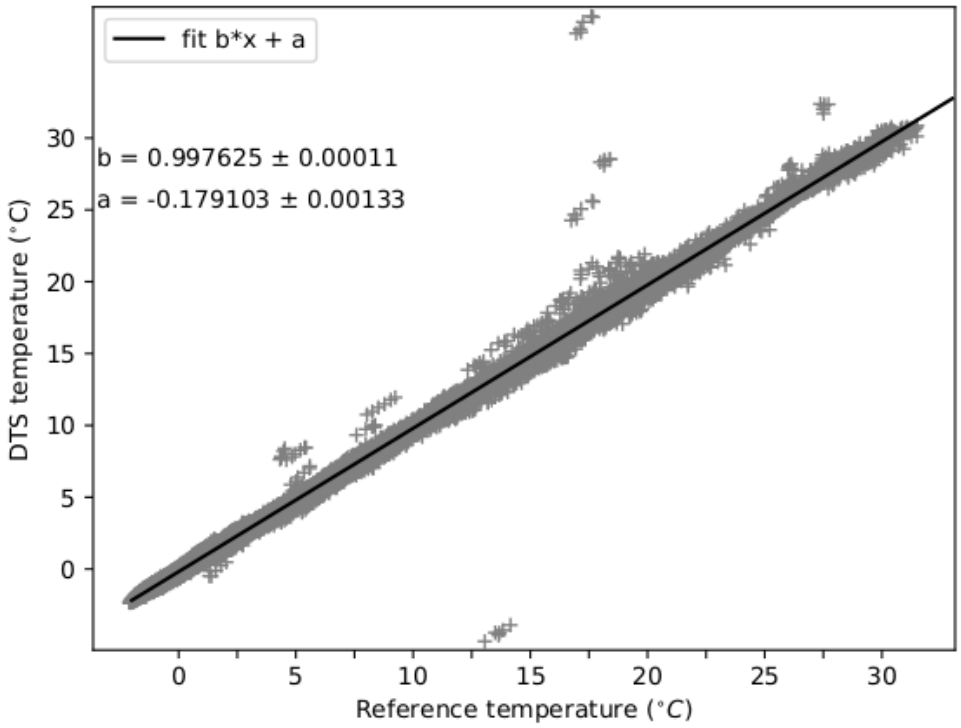

Figure 4.1: The comparison between the DTS temperatures and the reference measurements from heights 0.5, 1.5, 3.5, 6.0, 9.0, 12.5, 17.0 and 21.5 m. Both day- and nighttime measurements are included. A linear fit to the data is shown with black line and the parameters for the fit are shown in the upper left corner of the figure. In general, the fit is very close to 1/1, with DTS showing slightly lower temperatures on average. There are only few outliers that are clearly off the fitted line. The outliers were included in the fitting.

mistors were attached to the nearby tall mast at the same height as the optical fiber. The comparison between the DTS temperatures and the reference temperatures is shown in figure 4.1. There are some points where the readings differ significantly from each other, but overall the DTS seems to measure temperatures with very good precision. The outliers that are way off the fitted line were very likely faulty and do not represent the performance of the DTS system, as they were unrealistic and appeared randomly in the middle of seemingly realistic temperature readings. The linear fit shows very close to 1/1 relation between DTS and the reference. Quite surprisingly the linear fit suggests that the DTS actually measured smaller temperatures on average than the reference thermistors. As already mentioned, DTS measurements are known to be affected by solar radiation and therefore overestimate the air temperature. The reasons for the results in figure 4.1 are not clear, but there are some possible explanations. Firstly, the reference thermistors and the DTS fiber were not measuring at exactly the same place, only at the same height. Secondly, the reference thermistors can possibly be affected by solar heating.

4.2 Stability within the canopy

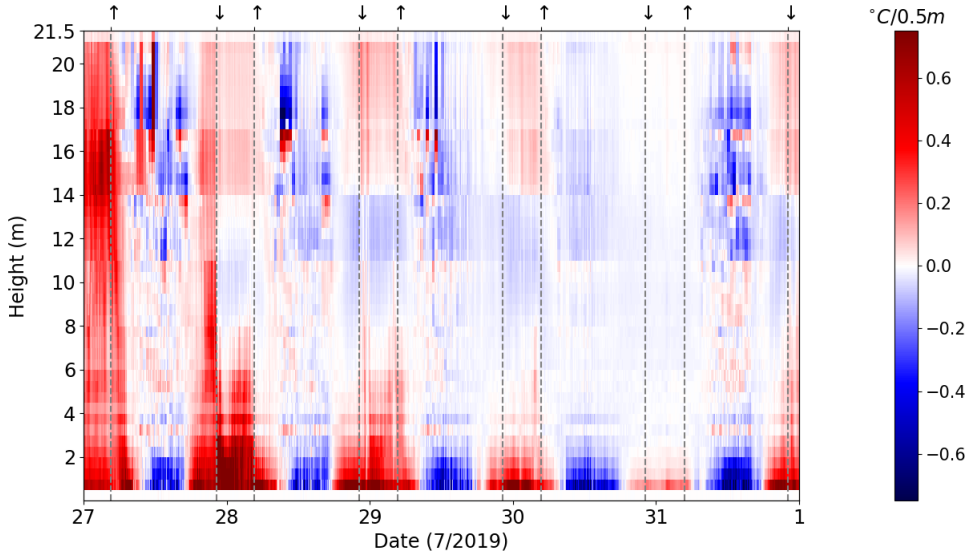

Figure 4.2: Vertical temperature gradient during the end of July 2019. Red color indicates temperature rising with height (inversion). Blue color indicates that the temperature decreases with height. The gradient is calculated separately between each adjacent point. The darker the color is, the larger is the temperature gradient. Y-axis shows the measurement height and x-axis shows the date, with the date numbers at midnight. Sunset and sunrise times are shown with black dashed lines and arrows pointing down and up, respectively.

For the analysis the vertical temperature gradient was plotted for each averaging period. Figure 4.2 shows an example of the observed temperature gradients in the end of July 2019. The mean and standard deviation of the observed potential temperature difference between 1 m and 20 m during nighttime was 0.74 ± 1.05 °C, so on average it seems that the canopy layer is relatively weakly stable. That said, many nights with clear skies and weak winds had static stabilities of over 5 °C, with the maximum observed value being 6.2 °C. The beginning of 27th of July and partly also between 27th and 28th of July showed a strong inverse temperature gradient that spanned all the way from the ground to over the canopy top at approximately 17 m height. The temperature gradient during the night between 28th and 29th of July appeared to be a very typical example during the measurement period. There are two notable temperature inversions: one strong inversion shown with dark red color that reaches from the ground to about 8-10 meters height, and the other, a bit weaker inversion that spans from 14 meters to over the top of the canopy shown in lighter red color. During some nights, the temperature inversion was very weak or completely absent. A good example of this is the beginning of 31st of July, during which the temperature was very close to constant in the vertical. The almost constant temperature profile is seen as near-white color in figure 4.2.

4.2.1 Calculated depth of SBL

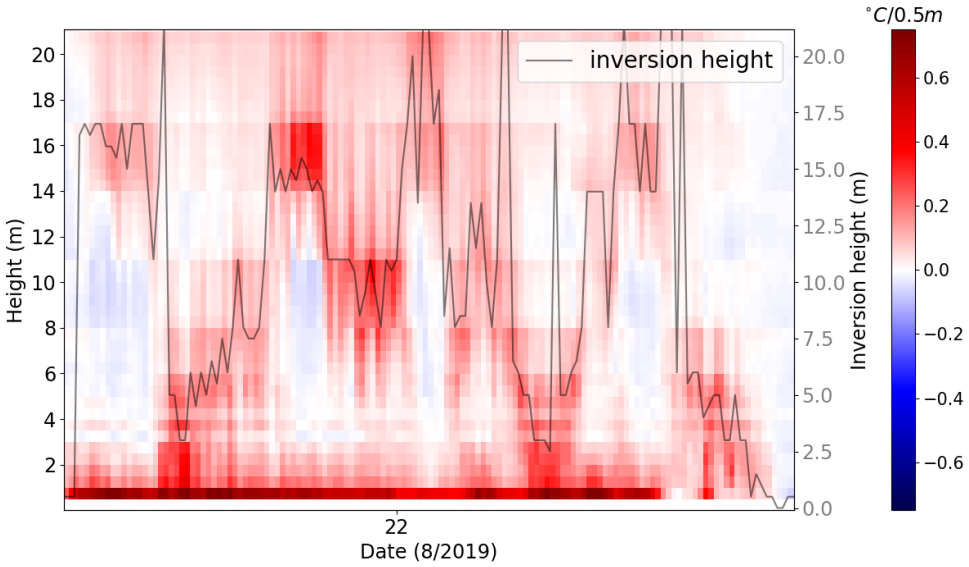

Figure 4.3: An example night in August 2019 that shows the performance of the method for determining the depth of SBL. The colors and axes are the same as in figure 4.2. The calculated depth of SBL is marked with a grey line.

In order to find out how katabatic wind and the height of the temperature inversion are connected, the depth of SBL had to be calculated. The depth of SBL was set at the height of the largest standard deviation of temperature. Also a minimum requirement of 0.2 °C for the standard deviation was set to filter the weakest inversions and noise from the results. If the gradient was less than the threshold value, the inversion was assumed to be negligibly weak and ignored.

From figure 4.3, it can be seen that the selected method is able to find the top of the inversion quite well in most cases. However, the method has potential for improvements. As can be seen in figure 4.3, Some ”noise” in the calculated depth of SBL exists, meaning that the calculated depth is not smooth and includes unrealistic jumps, even if on average the curve follows the inversion well. Conditions with two separate inversion layers (seen in figure 4.2) were also challenging. In these cases, the height was selected based on the higher inversion layer. This kind of situation can be seen in figure 4.3 when there is red color at the bottom of the figure indicationg surface inversion, then blue color above and another red inversion layer on top of that. The calculated SBL depth is seen to follow the higher inversion layer.

The mean and standard deviation of the calculated SBL depth during nighttime were 1.90 ± 4.94 m. The result suggests that the stable layer mostly forms well within the open trunk space near the surface, but the deviation is large and it was not uncommon to observe the canopy layer to be stably stratified all the way to the top. The results

coincide well with the observations of average static stability. As it was relatively weak, the stable layer is not expected to develop to its full depth, but to remain shallow. This result can be taken as evidence of the SBL depth calculations providing reliable results on average.

4.2.2 Effect of environmental conditions

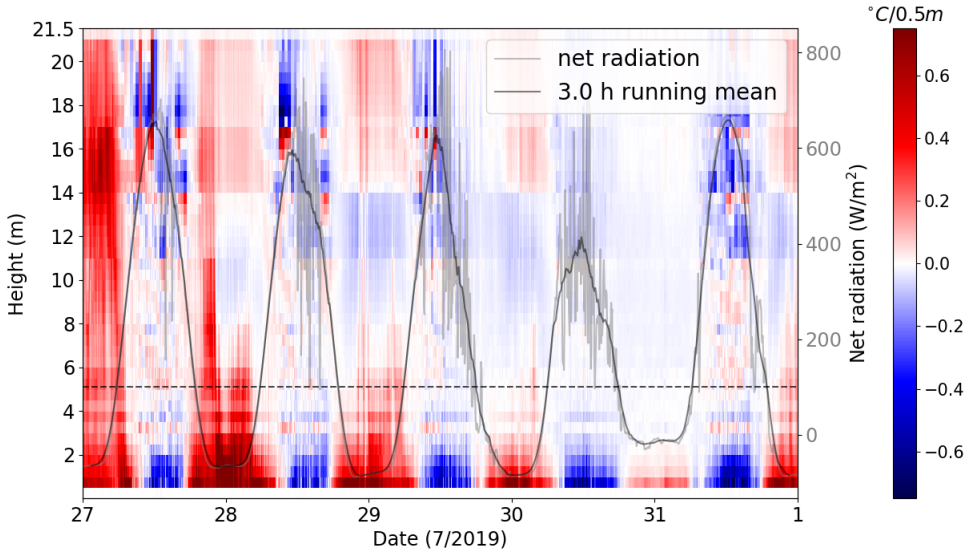

Figure 4.4: Vertical temperature gradient in the same way as in figure4.2 and net radiation above the canopy at the end of July 2019. Dark grey curve shows the 3-hour running mean of net radiation. Black dashed line marks net radiation of 100 W/m^2.

The temperature gradient within the canopy was compared against various environmental factors. These factors include wind above the canopy at 33.6 m, wind shear between 33.6 m and 8.4 m, friction velocity above the canopy at 23.3 m and net radiation at 23.3 m.

Generally, strong wind and wind shear was found to suppress the formation of strong temperature inversion within the canopy. However, net radiation was found to dominate the formation of stable layer during nighttime, even when wind or friction velocity was relatively strong.

Figure 4.4 shows the vertical temperature gradient within the canopy and net radiation above the canopy. Net radiation was the most important driving force to the formation of stable stratification. From figure 4.4 it can be seen, that when net radiation falls below about 100 W/m^2 before the sunset, a stable layer begins to form near the surface. During the early morning, as net radiation exceeds 100 W/m^2, the stable layer starts to dissipate.

4.3 Katabatic flow within the canopy

4.3.1 Flow direction

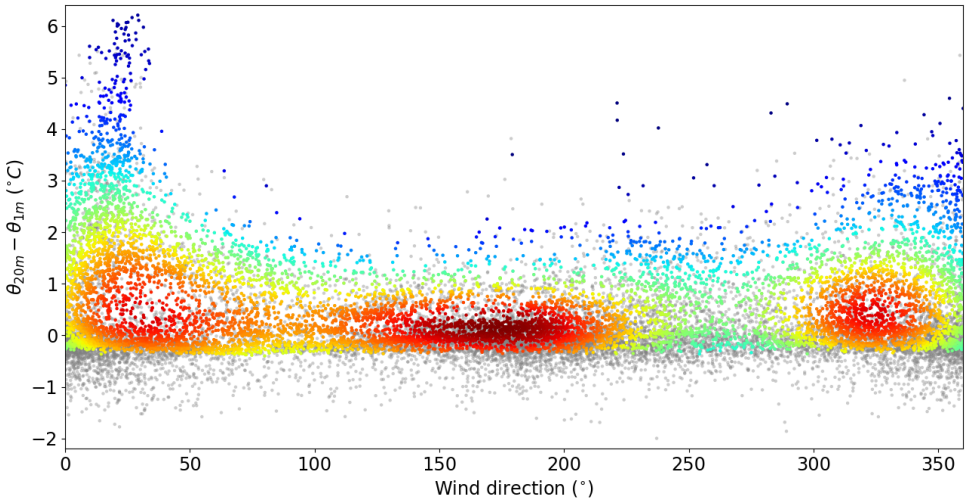

Figure 4.5: Scatter plot of the measured wind direction at 1 m height and the static stability of the canopy layer (potential temperature difference between 1 m and 20 m) during June-October 2019. This plot includes both daytime and nighttime winds. Grey dots are daytime data and colored dots are nighttime data. Color is used to show areas with the largest density of data points. Dark blue is less dense, light blue, yellow and red indicate greater densities.

The direction of the wind measured at 1 m height was plotted against the static stability of the canopy layer. Figure 4.5 shows their dependence when all times, days and nights, were considered. The dominant wind direction seems to be 150°-200°, with another maxima around 360° (northerly wind). Higher stabilities seem to coincide with the northerly wind maxima.

During the day, the canopy layer is often unstable, which can be seen from the grey daytime dots in figure 4.5. They lie mostly in area of negative static stability. Northerly winds are observed more commonly during highly stable conditions, which often coincides with nighttime. The middle wind direction maximum from figure 4.5 still remains quite strong during nighttime, although it does not coincide with highly stable conditions.

The remaining of the more southern maximum also in the nighttime data indicates, that the categorization of the winds to ”sun over the horizon” and ”sun below the horizon” is possibly not enough to completely separate the slope-dependent nocturnal flow from the slope-independent flow. One possible reason for this is that the stability is not strong enough just after sunset or just before sunrise for the slope-dependent flow to dominate. However, it is still clear that the more stable the canopy layer is, the more the wind near the surface is directed along the slope from north to south.

4.3.2 Flow speed

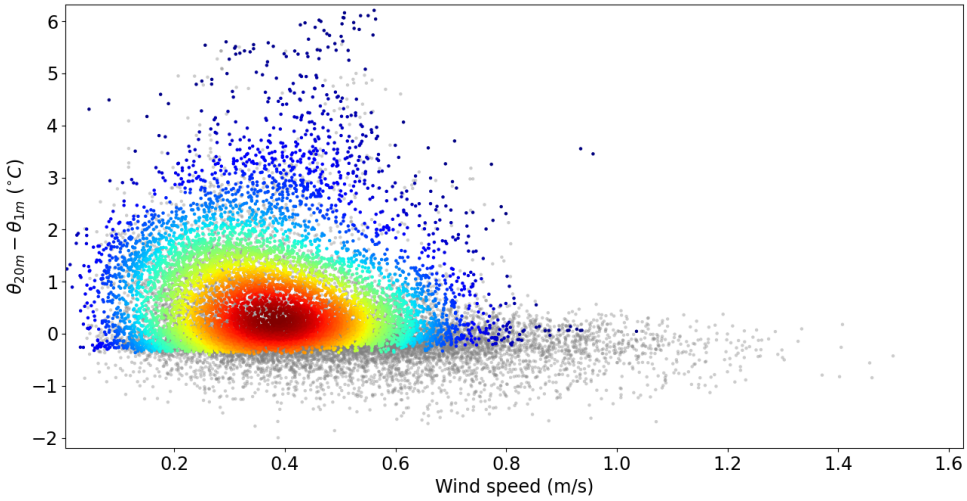

Figure 4.6: Scatter plot of the measured wind speed at 1 m height and the static stability of the canopy layer (potential temperature difference between 1 m and 20 m) during June-October 2019. Both daytime and nighttime winds are included in this plot. Grey dots are daytime data and colored dots are nighttime data. Color indicates the density of data points, blue is less dense, yellow is denser and red is the densest.

Figure 4.6 shows the distribution of the measured flow speeds at 1 m height as a function of static stability within the canopy layer when both day- and nighttime are taken into account. The distribution shows that most of the flow speeds are under 0.75 m/s and almost all wind speeds during high stabilities fall under that limit. The most commonly observed wind speeds are about 0.4 m/s and they most commonly coincide with weakly stable canopy layer.

Considering only the daytime winds, the results again change noticeably just as they did in the case of the direction of the flow. As one would expect based on previous information about static stability (chapter 2.1.1), most of the unstable cases when the stability is <0 are observed during daytime. The strongest winds of over 1 m/s were observed only during daytime, when the air within the canopy was neutrally stratified or unstable.

Based on these results seen in figure 4.6, the tranformation of eddy kinetic energy to the kinetic energy of the wind near the surface in unstable situations might affect the wind speed more than stability does. Also, it is not reasonable to state that the katabatic flow strengthens with increasing stability, as the relation between the wind speed and stability is not very clear as the wind speed varies a lot regardless of stability. This was surprising as the wind speeds were expected to have more clear dependence on and increase with increasing stability. The reason behind this kind of behaviour of the katabatic flow is unclear and therefore requires more research in the future.

4.4 Vertical katabatic wind profiles

4.4.1 Wind speed and depth of SBL

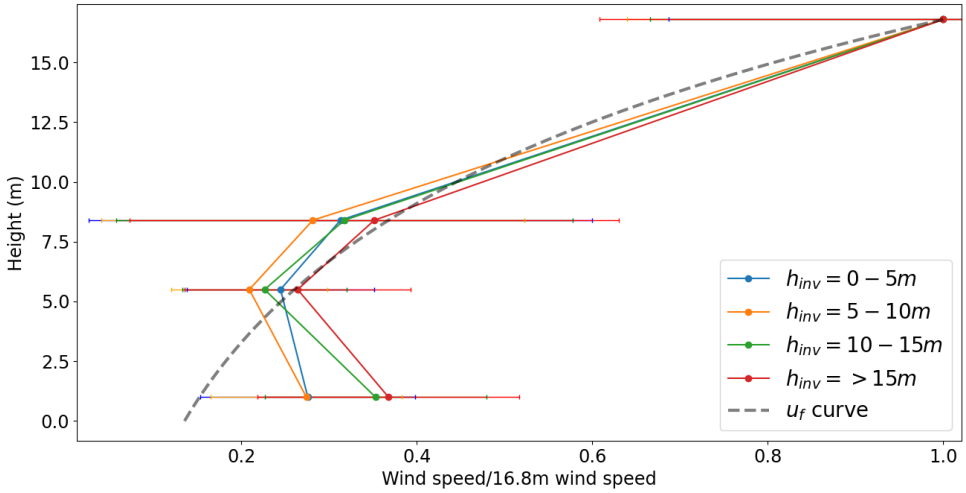

Figure 4.7: Average measured nighttime wind speed profile within the canopy binned by SBL depth. Y-axis shows height above ground. Grey dashed curve is the wind profile within the canopy predicted by Yi et al. (2005), which does not consider slope flows. The wind speed shown on the x-axis is normalized by the observed wind speed at the top of the canopy, 16.8 m.

The measured nighttime wind speeds below the canopy were divided into four bins by the calculated SBL depths and then averaged at each measurement height: 1 m, 5.5 m, 8 m and 16.8 m. The wind speeds were also normalized with the top-of-canopy (16.8 m) wind and then compared with the theoretical slope-independent wind presented in equation 2.16. Figure 4.7 shows, that the measured winds agreed with the theory well at over 8 m height, but below that they did differ from the theory. Between 8 m and 5 m the observed winds were on average less than the theory predicts, and below 5 m the winds were stronger than predicted by the theory. Standard deviation of the wind observations within the bins was relatively high, but still it is clear that the winds very close to the surface tend to get stronger than the widely used exponential model for wind within a canopy (equation 2.16) suggests.

4.4.2 Wind speed and stability

When the bin averaging was done with respect to different stabilities, the resulting average wind profiles look very similar to the winds binned by depth of SBL. This can be seen in figure 4.8. Difference to figure 4.7 is that the wind in especially the most stable bin deviates even more from the theoretical approximation.

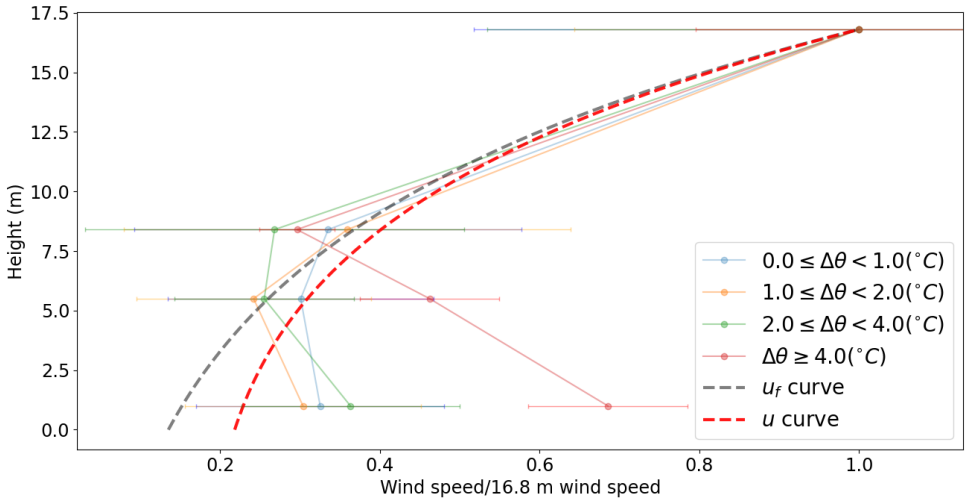

Figure 4.8: Same as in figure 4.7, but the winds are binned by the static stability of the canopy layer (potential temperature difference between 1 m and 20 m). Grey dashed curve shows the theoretical wind profile by Yi et al. (2005) without the slopewise component u_g. Red dashed curve shows the theoretical wind profile calculated according to equation 2.13, normalized by the wind speed at top of the canopy. The measured wind profiles are made more transparent to improve visibility of the theoretical profiles.

When the potential temperature gradient within the canopy layer is over four degrees, the measured winds at 1 m were on average 70 % of the wind at top of the canopy. The less stable bins have winds up to about 30 % of the wind at top of the canopy, which is similar to the wind binned by depth of SBL (figure 4.7). Based on figures 4.7 and 4.8, it seems that the katabatic flow speed near the ground is only weakly affected by depth of SBL and that it is more affected by the strength of the stability. This result was against expectations and should be interpreted carefully: further research is needed to establish a better understanding on how the depth of the stable layer affects katabatic flows.

4.4.3 Comparison between measurements and simplified theory

The observed wind profiles were compared with the complete form of the wind profile under the canopy shown in equation 2.13. The slopewise component u_g was calculated according to equation 2.15. In order to calculate the slopewise component as a function of height, the ambient temperature and the vertical potential temperature gradient within the canopy were set as constant 15 °C and 6 °C, respectively, to represent a typical strongly stable nocturnal canopy layer observed during the measurement campaign. From figure 4.8 it can be seen, that the theoretical model by Yi et al. (2005) cannot produce as strong katabatic flow near the ground as was observed even during weakly stable conditions. In the theoretical model the low level wind within the canopy is increased slightly when compared to the model without the slopewise component, but the increase is much smaller than observed.

The theoretical wind profile by Yi et al. (2005) assumes, that the one-sided leaf area index LAI as well as the drag coefficient C_D of the canopy elements such as trunks, leafs and branches are constant inside the canopy. These assumptions are not valid in reality. The leaf area of the forest is not uniform but more concentrated towards the top of the canopy, while the bottom part of the canopy has relatively open trunk space with very little leaf area. When LAI is not really uniform in the vertical direction, also C_D cannot be constant in the vertical direction. It is very likely that the open trunk space has smaller drag coefficient than the layer above where the majority of the branches and therefore the majority of leaf area is. The smaller drag near the surface could explain why the model produces much weaker wind near the surface than is actually observed.

5. Conclusions

The aim of this study was to find how the within-canopy katabatic flows at SMEAR-II station in Hyytiälä, southern Finland depend on the depth of the stable layer and the static stability within the canopy. The vertical profile of temperature within a boreal forest canopy was studied using distributed temperature sensing (DTS) system in Hyytiälä, southern Finland during July-October 2019. The temperature was measured with a vertical resolution of 0.5 m between heights 0-21.5 m and with a horizontal resolution of 0.127 m.

The temperature profile was compared with wind speed and direction measured within the canopy at 1 m, 5.5 m, 8 m and 16.8 m. The observed winds were compared with the static stability and the height of the temperature inversion within the canopy layer in order to find out how the temperature profile affects the sub-canopy airflow. The observed winds were also compared with a theoretical model for wind inside a forest canopy to see how well the theory represents the observed conditions.

The height of the temperature inversion was computationally estimated as the height of the maximum standard deviation of the temperature. If the standard deviation did not exceed a minimum value of 0.2 °C, the inversion was taken as negligibly weak. This approach was able to follow the height of the inversion well in most cases. The method produced some unrealistic jumps in the SBL depth estimation, but the values were still realistic. Also situations with two separate inversion layers separated by a neutral or weakly stable layer were challenging for the method used. In these cases, the inversion height followed the higher inversion layer.

The dominant direction for the sub-canopy wind was found to be around 150°-200°. The sub-canopy wind direction was found to turn more northerly (0°$\pm$ 50°) during nighttime, when a temperature inversion formed within the canopy layer. The slope of the terrain in Hyytiälä is aligned approximately in north-south direction, so this is a sign of a katabatic downslope flow developing at the measurement site during stable nights.

The observed flow speeds shown in figure 4.6 were found to be mostly < 1 m/s at 1 meters above the ground, with most of the observed wind speeds around 0.25-0.75 m/s. The peak winds during daytime were slightly stronger than during nighttime and the strongest measured winds were about 1.5 m/s. One of the objectives of this study

was to find how the wind speed near the ground is related to the static stability of the canopy layer. No clear relationship was found between them, as the wind speed did not clearly change in either direction with respect to the stability.

The wind speed within the canopy was compared to an exponential model for wind within a canopy (equation 2.16). The observations show that the depth of the stable layer does not affect the vertical wind profile by much, as the changes in wind speeds were well inside the standard deviation of the measurements. However, the model seems to underestimate the wind speed at the base of the canopy layer between 1-5 meters with all stable layer depths.

Similarly, the average wind vertical profiles during various levels of stability were compared against a simplified theoretical model which did not consider slope flows or below-canopy stability on wind profiles. The analysis showed that the theory underestimates the wind speed more and more with increasing stability. In the strongest observed stable conditions the wind speed was much higher at 1-8 meters, and in weakly stable conditions the wind speed was still higher than predicted at 1-5 meters, although by lesser margin than in the strongly stable case. When the slope flows were included in the model and the theoretical wind profile compared to the measurements, the difference between observed and modelled winds got smaller but modelled wind still greatly underestimated the observed wind speeds. The model assumes that the drag coefficient (C_D) and all-sided leaf area index (LAI) are constants in the vertical direction, which are not valid assumptions at the measurement site. The difference between the modelled and real distribution of C_D and LAI most likely is an important reason why the model underestimates wind speed near the bottom of the canopy layer.

The results of this study concerning the relationship between the vertical profile of wind and static stability within the canopy agree with a previous study at the same measurement site by Launiainen et al. (2007). However, Launiainen et al. (2007) state that the wind profile inside the canopy layer is logarithmic even close to the ground. In this study, the wind profile was not observed to be logarithmic in stable conditions. That said, the results have to be interpreted with caution as the method used to determine the SBL depth introduces potential error for the analysis. The standard deviation of temperature was found to get its maximum value close to the top of the inversion layer, but the method did not work perfectly. Also the definition of daytime and nighttime winds based on sunset and sunrise times might not be the ideal solution to separate katabatic flow from the measurements. This is why further development of methods to define the height of the inversion layer and the nocturnal katabatic flow would potentially be very beneficial in future analyses on this subject.

Alekseychik et al. (2013) studied the evolution of the nocturnal stable canopy layer in Hyytiälä, Finland. They found that the formation of a stable canopy layer starts as

a thin layer at the surface on clear and calm evenings, when the trunkspace gets stably stratified. If cloudiness or wind does not disturb the stable layer, also the upper part of the canopy layer where the majority of the leaf area is gets stably stratified. The results concerning the formation of the nocturnal stable layer agree with the results of this study. However, Alekseychik et al. (2013) concluded that the katabatic flow that forms when the canopy is stably stratified tends to be stronger in a deeper stable layer. This study could not confidently find the same relationship between the depth of the stable layer and the strength of the katabatic flow, although the results were not against that either. Considering EC flux measurements, it is clear that the slopewise flow forming in stably stratified conditions within a forest canopy is an issue that needs to be taken into account so that the flux measurements can yield reliable results when used in sloping terrain. To improve EC data interpretation, the structure and dynamics of stably stratified, sloping canopy layers still need to be investigated further.

Acknowledgements

First I want to thank my supervisor Olli Peltola for all the insightful advice during the data analysis and writing process of this thesis work. Thank you for being such a supportive supervisor during the time I worked with my thesis and also thank you for giving me the chance to work with you also in Sodankylä during 2020.

Secondly, thanks to my supervisor Timo Vesala for your comments and guidance during this thesis work. Your feedback really helped me to keep confident about my thesis work. I did not expect that we would be connected by my thesis work when I first encountered you in Hyytiälä in 2019, but it is great that it happened. Special thanks go to all the fellow meteorology students whose company made the whole studying experience unforgettable.

Lastly, I want to thank my family for giving me all the support at home and being there for me no matter what.

Bibliography

Albini, F. A. A. (1981). Phenomenological model for wind speed and shear stress profiles in vegetation cover layers. *J. Appl. Meteorol.*, 20, 1325–1335.

Alekseychik, P., Mammarella, I., Launiainen, S., Rannik, Ü. and Vesala, T. (2013). Evolution of the nocturnal decoupled layer in a pine forest canopy. *Agr. Forest. Meteorol.*, 174, 15–27.

Aubinet, M., Heinesch, B. and Yernaux, M. (2003). Horizontal and vertical CO_2 advection in a sloping forest. *Boundary-Layer Meteorol.*, 108, 397–417.

Aubinet, M., Vesala, T. and Papale, D. (2012). *Eddy covariance: a practical guide to measurement and data analysis.* Springer Atmospheric Sciences.

Baas, P., Steeneveld, G., van de Weil, B. and Holtslag, A. (2006). Exploring self-correlation in the flux-gradient relationships for stably stratified conditions. *J. Atmos. Sci.*, 63, 3045–54.

Baldocchi, D. D. and Meyers, T. P. (1991). Trace gas exchange at the floor of a deciduous forest I. Evaporation and CO_2 efflux. *J. Geophys. Res.*, 96, 7271–7285.

Bianco, L., Djalalova, I., King, C. and Wilczak, J. (2011). Diurnal evolution and annual variability of boundary-layer height and its correlation to other meteorological variables in California's Central Valley. *Bound.-Lay. Meteorol.*, 140, 491–511.

Bossert, J. E. and Cotton, W. R. (1994). Regional-scale flows in mountain terrain. Part I: A numerical and observational comparison. *Mon. Wea. Rev.*, 122, 1449–1471.

Bosveld, F., van Ulden, A. and Beljaars, A. (1999). A comparison of ECMWF re-analysis data with fluxes and profiles observed in Cabauw. *Re-Analysis (ERA) Project Report, ERA-15 Project Report Series No. 8.* ECMWF.

Bosveld, F., de Bruin, E. and Holtslag, A. A. (2008). Intercomparison of single-column models for GABLS 3: Preliminary results. paper presented at 18th AMS Workshop on Boundary Layer and Turbulence, *Am. Meteorol. Soc.*, Stockholm, Sweden.

Boubel, R. W., Fox, D. L., Turner, D. B. and Stern, A. C. (1994). *Fundamentals of Air Pollution*, Academic Press, 574 pp.

Brown, A., Beljaars, A., Hersbach, H., Hollingsworth, A., Miller, M. and Vasiljevic, D. (2005). Wind turning across the marine atmospheric boundary layer. *Q. J. R. Meteorol. Soc.*, 131, 1233–1250.

Brown, A., Beare, R. J., Edwards, J. M., Lock, A. P., Keogh, S. J., Milton, S. F. and Walters, D. N. (2008). Upgrades to the boundary-layer scheme in the met office numerical weather prediction model. *Boundary-Layer Meteorol.*, 128, 117–132.

Carlson, M. A. and Stull, R. B. (1986). Subsidence in the nocturnal boundary layer. *J. Clim. Appl. Meteorol.*, 25(8), 1088–1099.

Cionco, R. M. (1965). A mathematical model for air flow in a vegetation canopy. *J. Appl. Meteorol.*, 4, 517–522.

Cionco, R. M. (1972). A wind-profile index for canopy flow. *Boundary-Layer Meteorol.*, 3, 255–263.

Cowan, I. R. (1968). Mass, heat, and momentum exchange between stands of plants and their atmospheric environment. *Q. J. R. Meteorol. Soc.*, 94, 318–332.

Cuxart, J. et al. (2006). Single-column model intercomparison for a stably stratified atmospheric boundary layer. *Boundary-Layer Meteorol.*, 118, 273–303.

Cushman-Roisin, B. (2019). *Environmental Fluid Mechanics.* John Wiley & Sons, Inc.

Feigenwinter, C., Bernhofer, C. and Vogt, R. (2004). The influence of advection on the short term CO_2 -budget in and above a forest canopy. *Boundary-Layer Meteorol.*, 113, 201–224.

Finnigan, J., Ayotte, K., Harman, I., Katul, G., Oldroyd, H., Patton, E., Poggi, D., Ross, A. and Taylor, P. (2020). Boundary-layer flow over complex topography. *Bound.-Layer Meteor.*, 177, 247–313.

Finnigan, J. (2008). Introduction to flux measurements in difficult conditions. *Ecol. Appl.*, 18, 1340–1350.

Finnigan, J. (2000). Turbulence in plant canopies. *Agric. For. Meteorol.*, 32, 519–571.

Gao, W., Shaw, R. H. and Paw U, K. T. (1989). Observation of organized structure in turbulent flow within and above a forest canopy. *Boundary-Layer Meteorol.*, 47, 349–377.

Garratt, J. R. (1994). Review: the atmospheric boundary layer. *Earth-Science Reviews*, 37(1994), 89–134.

Dakin, J. P., Pratt, D. J., Bibby, G. W. and Ross, J. (1985). Distributed optical fiber Raman temperature sensor using a semiconductor light-source and detector. *Electron. Lett.*, 21(13), 569–570, doi:10.1049/el:19850402.

Inoue, E. (1963). On the turbulent structure of air flow within crop canopies. *J. Meteorol. Soc. Jpn.*, 41, 317–326.

de Jong, S. A. P., Slingerland, J. D. and van de Giesen, N. C. (2015). Fiber optic distributed temperature sensing for the determination of air temperature. *Atmos. Meas.Tech.*, 8, 335–339, https://doi.org/10.5194/amt-8-335-2015, https://www.atmos-meas-tech.net/8/335/2015/.

Kaimal, J. C. and Finnigan, J. J. (1994). *Atmospheric Boundary Layer Flows: Their Structure and Measurement*. Oxford University Press.

Keller, C. A., Huwald, H., Vollmer, M. K., Wenger, A., Hill, M., Parlange, M. B. and Reimann, S. (2011). Fiber optic distributed temperature sensing for the determination of the nocturnal atmospheric boundary layer height. *Atmos. Meas. Tech.*, 4, 143–149, doi:10.5194/amt-4-143-2011.

Koehler, M., Ahlgrimm, M. and Beljaars, A. (2011). Unified treatment of dry convective and stratocumulus-topped boundary layers in the ECMWF model. *Q. J. R. Meteorol. Soc.*, 137, 43–57.

Kurashima, T., Horiguchi, T. and Tateda, M. (1990). Distributed-temperature sensing using stimulated Brillouin-scattering in optical silica fibers. *Opt. Lett.*, 15(18), 1038–1040.

Launiainen, S., Vesala, T., Mölder, M., Mammarella, I., Smolander, S., Rannik, Ü., Kolari, P., Hari, P., Lindroth, A. and Katul, G. G. (2007). Vertical variability and effect of stability on turbulence characteristics down to the floor of a pine forest. *Tellus B: Chemical and Physical Meteorology*, 59:5, 919–936, DOI: 10.1111/j.1600-0889.2007.00313.x.

Lied, N. T. (1964). Stationary hydraulic jump in a katabatic flow near Davis, Antarctica, 1961. *Aust. Meteor. Mag.*, 47, 40–51.

Macdonald, R. W. (2000). Modelling the mean velocity profile in the urban canopy layer. *Boundary-Layer Meteorol.*, 97, 25–45.

Mahrt, L. (1982). Momentum balance of gravity flows. *J. Atmos. Sci.*, 39, 2701–2711.

Mahrt, L. (1990). Relation of slope winds to the ambient flow over gentle terrain. *Bound.-Layer Meteor.*, 53, 93–102.

Mahrt, L. (2014). Stably stratified atmospheric boundary layers. *Annu. Rev. Fluid Mech.*, 46, 23–45.

Mahrt, L., Lee, X., Black, A., Neumann, H. and Staebler, R. M. (2000). Nocturnal mixing in a forest subcanopy. *Agric. For. Meteorol.*, 101, 67–78.

Massman, W. J. (1987). A comparative study of some mathematical models of the mean wind structure and aerodynamic drag of plant canopies. *Boundary-Layer Meteorol.*, 40, 179–197.

Mohan, M. and Tiwari, M. K. (2004). Study of momentum transfer within a vegetation canopy. *Proc. Indian Acad. Sci. Earth Planet. Sci.*, 113, 67–72.

Monti, P., Fernando, H. J. S., Princevac, M., Chan, W. C., Kowalewski, T. A. and Pardyjak, E. R. (2002). Observations of flow and turbulence in the nocturnal boundary layer over a slope. *J. Atmos. Sci.*, 59, 2513–2534.

Nieuwstadt, F. T. M. (1984). The turbulent structure of the stable, nocturnal boundary layer. *J. Atmos. Sci.*, 41, 2202–2216.

Papadopoulos, K. H. and Helmis, C. G. (1999). Evening and morning transition of katabatic flows. *Bound.-Layer Meteor.*, 92, 195–227.

Papale, D., Reichstein, M., Aubinet, M., Canfora, E., Bernhofer, C., Kutsch, W., Longdoz, B., Rambal, S., Valentini, R., Vesala, T. and Yakir, D. (2006). Towards a standardized processing of Net Ecosystem Exchange measured with eddy covariance technique: algorithms and uncertainty estimation. *Biogeosciences*, 3, 571–583.

Parish, T. R. and Bromwich, D. H. (1989). Instrumented aircraft observations of the katabatic wind regime near Terra Nova Bay. *Mon. Weather Rev.*, 117, 1570–1585.

Peltola, O., Lapo, K., Martinkauppi, I., O'Connor, E., Thomas, C. K. and Vesala, T. (2020). Suitability of fiber-optic distributed temperature sensing to reveal mixing processes and higher-order moments at the forest-air interface. *Atmos. Meas. Tech. Discuss.* [preprint], https://doi.org/10.5194/amt-2020-260, in review.

Petrides, A. C., Huff, J., Arik, A., Van de Giesen, N., Kennedy, A. M., Thomas, C. K. and Selker, J. S. (2011). Shade estimation over streams using distributed temperature sensing. *Water Resour. Res.*, 47, W07601, doi:10.1029/2010WR009482.

Raupach, M. R. and Thom, P. G. (1981). Turbulence in and above plant canopies. *Annu. Rev. Fluid Mech.*, 13, 97–129.

Sandu, I., Beljaars, A., Bechtold, P., Mauritsen, T. and Balsamo, G. (2013). Why is it so difficult to represent stably stratified conditions in numerical weather prediction (NWP) models? *J. Adv. Model. Earth Syst.*, 5, 117–133.

Schilperoort, B., Coenders-Gerrits, M., Luxemburg, W., Jiménez Rodríguez, C., Cisneros Vaca, C. and Savenije, H. (2018). Technical note: Using distributed temperature sensing for Bowen ratio evaporation measurements. *Hydrol. Earth Syst. Sci.*, 22, 819–830, https://doi.org/10.5194/hess-22-819-2018.

Seibert, P., Beyrich, F., S.-E. Gryning, S.-E., Joffre, S., Rasmussen, A. and Tercier, P. (2000). Review and intercomparison of operational methods for the determination of the mixing height. *Atmos. Environ.*, 34, 1001–1027.

Selker, J. S., Thévenaz, L., Huwald, H., Mallet, A., Luxemburg, W., van de Giesen, N., Stejskal, M., Zeman, J., Westhoff, M. and Parlange, M. B. (2006). Distributed fiber-optic temperature sensing for hydrologic systems. *Water Resour. Res.*, 42, W12202, doi:10.1029/2006WR005326.

Smedman, A. S., Tjernström, H. and Högström, U. (1993). Analysis of the turbulence structure of a marine low-level jet. *Bound.-Layer Meteorol.*, 66, 105–26.

Sorbjan, Z. (2010). Gradient-based scales and similarity laws in the stable boundary layer. *Q. J. R. Meteorol. Soc.*, 136, 1243–1254.

Staebler, R. M. and Fitzjarrald, D. R. (2004). Observing subcanopy CO_2 advection. *Agric. For. Meteorol.*, 122, 139–156.

Stiperski, I., Holtslag, A. A. M., Lehner, M., Hoch, S. W. and Whiteman, C. D. (2020). On the turbulence structure of deep katabatic flows on a gentle mesoscale slope. *Q. J. R. Meteorol. Soc.*, 146, 1206–1231.

Sun, J., Jensen, N. O., Hummelshoej, P., Joergensen, H., Mahrt, L. and Chen, Z. (1998). Study of forest-atmospheric interaction over a beech forest. *Twenty-Third Conf. Agric. For. Meteorol.*, Am. Meteorol. Soc., Albuquerque, 47–51.

Svensson, G. and Holtslag, A. (2009). Analysis of model results for the turning of the wind and the related momentum fluxes and depth of the stable boundary layer. *Boundary-Layer Meteorol.*, 132, 261–277.

Tennekes, H. (1982). Similarity relations, scaling laws and spectral dynamics. *Atmospheric Turbulence and Air Pollution Modeling*, (Nieuwstadt, F. T. M. and van Dop, H., Eds.). Reidel, 37–68.

Thomas, C., Kennedy, A., Selker, J., Moretti, A., Schroth, M., Smoot, A., Tufillaro, N. and Zeeman, M. (2012). High-resolution fibre-optic temperature sensing: A new tool to study the two-dimensional structure of atmospheric surface-layer flow. *Bound.-Lay. Meteorol.*, 142, 177–192.

Tyler, S. W., Selker, J. S., Hausner, M. B., Hatch, C. E., Torgersen, T., Thodal, C. E. and Schladow, S. G. (2009). Environmental temperature sensing using raman spectra dts fiber-optic methods. *Water Resour. Res.*, 45, W00D23, doi:10.1029/2008WR007052.

Whiteman, C. D. (2000). *Mountain Meteorology: Fundamentals and Applications*. Oxford University Press, 355 pp.

Wilson, J. D., Ward, D. P., Thurtell, G. W. and Kidd, G. E. (1982). Statistics of atmospheric turbulence within and above a corn canopy. *Boundary-Layer Meteorol.*, 24, 495–519.

Wilson, N. R. and Shaw, R. H. (1977). A higher order closure model for canopy flow. *J. Appl. Meteorol.*, 16, 1197–1205.

Yi, C., Monson, R. K., Zhai, Z., Anderson, D. E., Lamb, B., Allwine, G., Turnipseed, A. A. and Burns, S. P. (2005). Modeling and measuring the nocturnal drainage flow in a high-elevation, subalpine forest with complex terrain. *J. Geophys. Res.*, 110, D22303.

Zilitinkevich, S. and Baklanov, A. (2002). Calculation of the height of the stable boundary layer in practical applications. *Bound.-Lay. Meteorol.*, 105, 389–409.